Realization of interlayer ferromagnetic interaction in $MnSb_2Te_4$ toward the magnetic Weyl semimetal state

Taito Murakami,[1] Yusuke Nambu,[2] Takashi Koretsune,[3] Gu Xiangyu,[1] Takafumi Yamamoto,[1]
Craig M. Brown,[4] and Hiroshi Kageyama[1,5,*]

[1]*Department of Energy and Hydrocarbon Chemistry, Graduate School of Engineering, Kyoto University, Nishikyo-ku, Kyoto 615-8510, Japan*
[2]*Institute for Materials Research, Tohoku University, Sendai, Miyagi 980-8577, Japan*
[3]*Department of Physics, Tohoku University, Sendai, Miyagi 980-8578, Japan*
[4]*Center for Neutron Research, National Institute of Standards and Technology, Gaithersburg, Maryland 20899, USA*
[5]*CREST, Japan Science and Technology Agency, Kawaguchi, Saitama 332-0012, Japan*

(Received 24 May 2019; revised manuscript received 25 September 2019; published 4 November 2019)

Magnetic properties of $MnSb_2Te_4$ were examined through magnetic susceptibility, specific-heat, and neutron-diffraction measurements. As opposed to isostructural $MnBi_2Te_4$ with the antiferromagnetic ground state, $MnSb_2Te_4$ develops a spontaneous magnetization below 25 K. From our first-principles calculations on the material in a ferromagnetic state, the state could be interpreted as a type-II Weyl semimetal state with broken time-reversal symmetry. Detailed structural refinements using x-ray-diffraction and neutron-diffraction data reveal the presence of site mixing between Mn and Sb sites, leading to the ferrimagnetic ground state. With theoretical calculations, we found that the presence of site mixing plays an important role for the interlayer Mn-Mn ferromagnetic interactions.

DOI: 10.1103/PhysRevB.100.195103

I. INTRODUCTION

Topological semimetals (TSMs), characterized by crossings of valence and conduction bands in the momentum space, have brought exciting opportunities to explore properties that are unattainable in conventional semimetals or metals [1–5]. Dirac semimetal is the first experimentally confirmed TSM, where a fourfold degenerate Fermi point is topologically protected by time-reversal symmetry (TRS) as well as space-inversion symmetry (SIS). This type of material has been experimentally verified in systems including Cd_3As_2 and Na_3Bi [6–9]. The degeneracy at the Dirac point can be lifted by breaking of either symmetry, leading to the Weyl semimetal state. The resultant twofold degenerated Weyl points have a distinct chirality, resulting in an open arc surface state and chiral anomaly at high magnetic fields [9–11]. Weyl semimetals have been found in materials without SIS (e.g., NbP and TaAs) [12–14] or TRS (e.g., Mn_3Sn and $Co_3Sn_2S_2$) [15,16].

A new class of TSMs called "type-II TSMs" has recently been proposed from theoretical perspectives [17]. Unlike conventional type-I TSMs, Dirac cones in type-II TSMs are largely tilted along certain momentum directions, violating the Lorentz invariance [17]. The distinct band topology leads to extremely anisotropic magnetoresistance [17,18]. After the prediction of the type-II Weyl semimetal state in WTe_2, several compounds were shown as type-II Weyl semimetal without SIS, including $MoTe_2$, LaAlGe, and $TaIrTe_4$ [19–25]. On the other hand, the experimental study of TRS-broken type-II Weyl semimetal is rather scarce. A rare example is the layered bismuthide $YbMnBi_2$, where the canting of the Yb moment from the c axis was initially proposed to break the TRS, resulting in the type-II Weyl semimetal state [26]. Subsequent optical conductivity measurements in $YbMnBi_2$, however, failed to confirm the canted Yb moments [27]. More recently, LnAlGe (Ln = Ce, Pr) have been predicted as a TRS broken TSM with both type-I and type-II crossings [28].

Ternary tellurides MPn_2Te_4 (M = Ge, Sn, Pb, Mn and Pn = As, Sb, Bi) have a layered structure as shown in Fig. 1(a) [29–31]. $MnBi_2Te_4$ with magnetic ions was theoretically proposed to have an antiferromagnetic topological insulating state [32–36], which was later confirmed from experimental studies [35–37]. It was also predicted that this material becomes TRS broken type-II Weyl semimetal if Mn moments are aligned ferromagnetically [34], a situation that has not been observed experimentally. In this paper, we synthesized isostructural $MnSb_2Te_4$ and conducted magnetic susceptibility, specific-heat, and neutron-diffraction measurements. Unlike the previous theory on $MnSb_2Te_4$ showing the A-type antiferromagnetic state [38], a ferromagnetic component develops in $MnSb_2Te_4$ below 25 K. Density functional theory calculations suggest that $MnSb_2Te_4$ in a ferromagnetic state can be expected to be a TRS broken type-II Weyl semimetal. Structural refinements using x-ray-diffraction (XRD) and neutron-diffraction data, however, reveal the presence of site mixing between Mn and Sb sites, leading to the ferrimagnetic ground state. The effect of site mixing is investigated through first-principles calculations.

II. EXPERIMENTAL AND CALCULATION DETAILS

A polycrystalline sample of $MnSb_2Te_4$ was synthesized via the solid-state reaction. Mn, Sb, and Te (99.99%, Kojundo Chemical) were weighed in a stoichiometric ratio, mixed, and

*kage@scl.kyoto-u.ac.jp

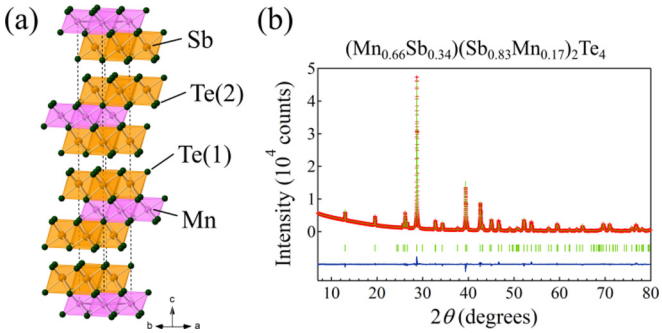

FIG. 1. (a) Crystal structure of $MnSb_2Te_4$. Pink, orange, and dark blue spheres represent Mn, Sb, and Te, respectively. Note that there are several antisite disorders between Sb and Mn sites. (b) Observed and calculated XRD patterns of $MnSb_2Te_4$. Red crosses and green and blue lines represent observed, calculated, and difference profiles. Green ticks are used to show the positions of the Bragg peaks.

pelletized in a nitrogen filled dry box. A pellet was sealed in an evacuated silica tube and heated up to 600 °C and kept for 10 h. Powder x-ray-diffraction experiments were performed using Bruker AXS D8 ADVANCE with Cu-$K\alpha$ radiation.

Dc magnetic susceptibility was measured by a commercial superconducting quantum interference device magnetometer (Quantum Design, MPMS) in the temperature range of 2–350 K under the magnetic field of 0–7 T. Specific heat C_{total} was measured by the relaxation method using a physical property measurement system (Quantum Design) down to 2 K. To estimate the lattice contribution C_{L}, we obtained the thermal variation of the Debye temperature $\theta_{\text{D}}(T)$ for the isostructural nonmagnetic analog $GeSb_2Te_4$ using the Debye equation. $\theta_{\text{D}}(T)$ of $MnSb_2Te_4$ was then estimated by multiplying a scaling factor according to $\theta_{\text{D}} \propto {M_0}^{-1/2}{V_0}^{-1/3}$, where M_0 and V_0 are the molar ratio mass and volume, respectively. C_{L} was obtained by converting the scaled $\theta_{\text{D}}(T)$ into specific heat. Detail of the analysis is provided in the Supplemental Material [39]. Electronic structure calculations were performed within the generalized gradient approximation using the Vienna *ab initio* simulation package [40,41].

Powder neutron-diffraction (PND) data were collected at 50 and 5 K using the high-resolution powder diffractometer BT-1 ($\lambda = 2.08$ Å) at the NIST Center for Neutron Research, USA. The obtained diffraction data were structurally refined using the JANA2006 [42] and FullProf Suite [43]. We employed group theoretical analysis to identify magnetic structures that are allowed by symmetry.

III. RESULTS AND DISCUSSIONS

Figure 1(b) shows the room-temperature XRD profile of the target compound. All the observed Bragg peaks can be indexed based on the rhombohedral unit cell. The lattice parameters of $a = 4.2385(3)$ Å and $c = 40.8497(3)$ Å are slightly smaller than those of $MnBi_2Te_4$ ($a = 4.334$ Å and $c = 40.910$ Å) [31], which is reasonable given the smaller ionic radius of Sb than that of Bi. Figure 1(a) displays the structure of $MnSb_2Te_4$ (space group $R3m$), with NaCl-type MnTe layers and tetradymite-type Sb_2Te_3 layers stacking

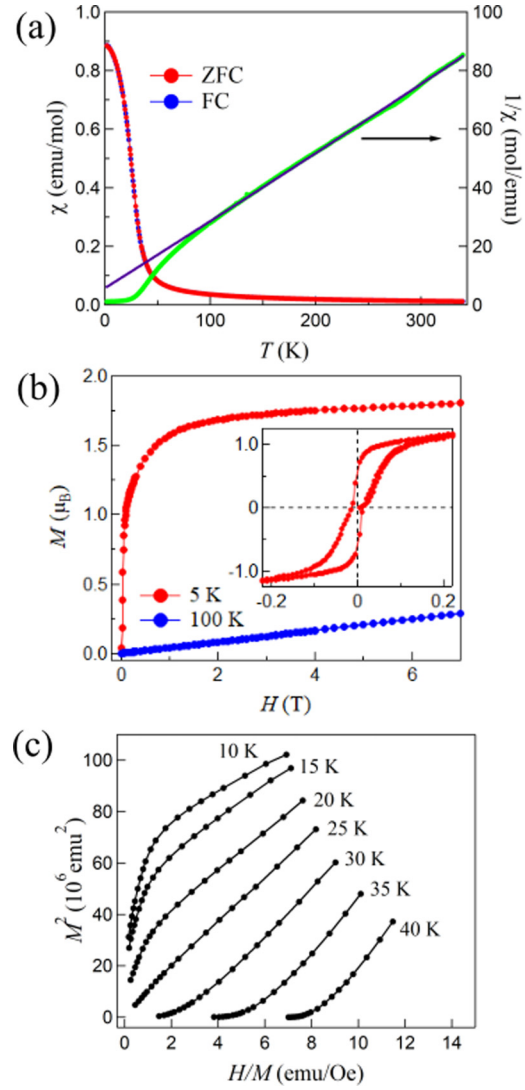

FIG. 2. (a) Left: Temperature dependence of magnetic susceptibility under an applied field of 0.1 T with zero-field cooling (red) and field cooling (blue) process. Right: Temperature dependence of inverse susceptibility. (b) Isothermal magnetization curves at 5 K (red) and 100 K (blue). The inset shows a hysteresis loop. (c) M^2 vs H/M (Arrott plot) at various temperatures around T_{C}.

alternatively along the c axis. The edge-shared $MnTe_6$ octahedral layer forms a regular triangular lattice. Since the formal valence is given by $(Mn^{2+})(Sb^{3+})_2(Te^{2-})_4$ and Mn^{2+} in a high-spin configuration has quenched the orbital degree of freedom, one can expect Heisenberg-type magnetic behavior in this material.

Eremeev *et al.* predicted that $MnSb_2Te_4$ has the A-type antiferromagnetic ground state, where the ferromagnetic Mn layers are stacked antiferromagnetically [38]. However, as shown in Fig. 2(a), the magnetic susceptibility of $MnSb_2Te_4$ in an applied field of 0.1 T rapidly increases below around 30 K, suggesting a transition to a ferromagnetic state (which, however, will be corrected later). From the Arrott plot [Fig. 2(c)], the transition temperature, T_{C}, is estimated to be 25 K, close to the Néel temperature of 24.2 K observed in $MnBi_2Te_4$ [35–37,44]. The isotherm magnetization curve at

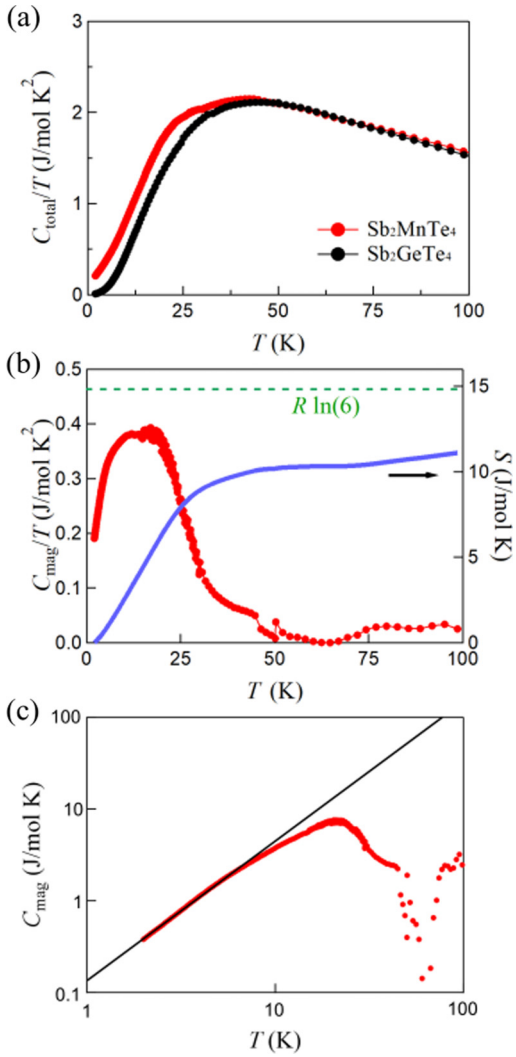

FIG. 3. (a) Temperature dependence of the specific heat divided by temperature. (b) Left: The magnetic part of the specific heat divided by temperature. Right: The magnetic entropy. The horizontal line indicates $R \ln 6$. (c) The magnetic part of the specific heat in full logarithmic scale.

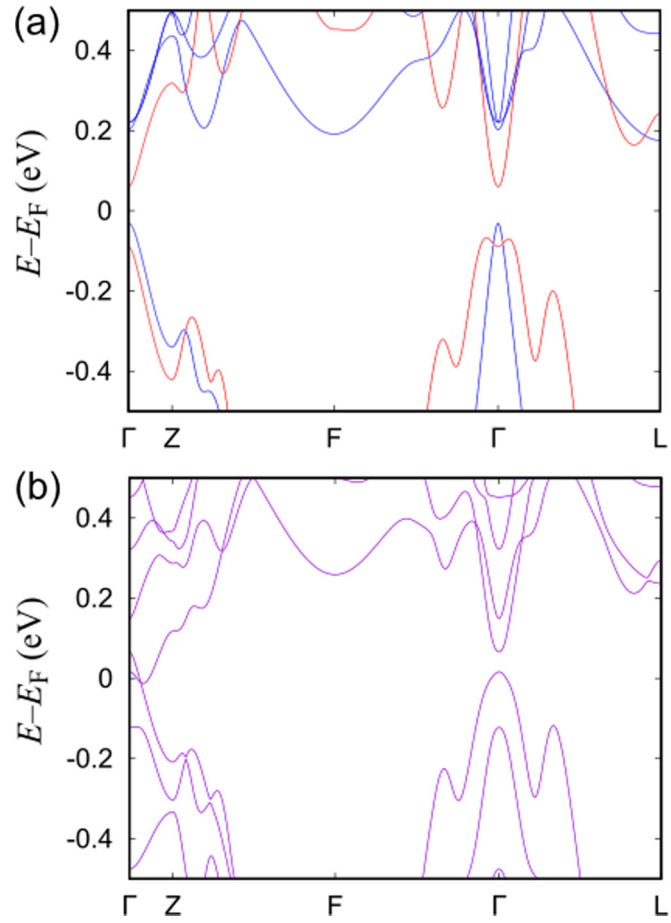

FIG. 4. Calculated band structures for $MnSb_2Te_4$ (a) without and (b) with SOC. In (a), the red (blue) color represents up-spin (down-spin) bands.

5 K up to 7 T [Fig. 2(b)] shows a small but finite ferromagnetic hysteresis loop. Such a small hysteresis has been sometimes reported in ferro- or ferrimagnets such as yttrium iron garnet [45]. The Curie-Weiss fitting yields the effective magnetic moment of $p_{\rm eff} = 5.842(7)\,\mu_{\rm B}$, in good accordance with the value expected from the high-spin state of Mn^{2+} ($5.92\,\mu_{\rm B}$). Figure S1 in the Supplemental Material [39] shows a difference in neutron data between $T = 5$ and 50 K. This clearly shows the increase of several nuclear reflections (e.g., 101 and 104) below $T_{\rm C}$, which is consistent with the ferromagnetic order with the magnetic wave vector $\boldsymbol{q}_{\rm m} = (0,\ 0,\ 0)$.

The magnetic transition is further probed by heat-capacity experiments. As shown in Fig. 3(a), the total specific heat $C_{\rm total}$ below 30 K is noticeably larger than that of the isostructural nonmagnetic $GeSb_2Te_4$, indicating the magnetic contribution to the specific heat. Its magnetic component $C_{\rm mag}$ is estimated by subtracting the lattice contribution from the data using $GeSb_2Te_4$ [Fig. 3(b), left axis]. Magnetic entropy, $S_{\rm mag}$, calculated from the integration of $C_{\rm mag}/T$ [Fig. 3(b), right axis], shows saturating behavior toward 30 K, followed by a gradual increase upon further warming. $S_{\rm mag}$ reaches about $11\,{\rm J/mol\,K^2}$ at 100 K, slightly smaller than the expected value of $R\ln 6$ for $S = 5/2$, where R is the gas constant. This observation implies that the short-range correlation persists well above $T_{\rm C}$. A power-law behavior in $C_{\rm mag} \propto T^{\alpha}$ with $\alpha = 1.52(1)$ is observed at temperatures below 10 K [Fig. 3(c)]. If there is a long-range magnetic order, α follows the relation of $\alpha = d/\upsilon$, where d is the dimensionality of the magnon excitation and υ is related to the type of the magnetic order ($\upsilon = 1$ and 2, respectively, stand for antiferromagnetic and ferromagnetic order). The observed $T^{3/2}$ dependence in $MnSb_2Te_4$ implies three-dimensional-like magnon excitations from a ferromagnetic state. However, the limited fitting range prevented us from further elucidation of the magnetic excitations.

As shown above, $MnSb_2Te_4$ undergoes a magnetic transition with a spontaneous magnetization, in contrast to the antiferromagnetic structure in $MnBi_2Te_4$ [36,37,44,46]. To obtain more insight into the ground state in $MnSb_2Te_4$, we performed first-principles calculations assuming a ferromagnetic state with an out-of-plane easy axis. Without the spin-orbit coupling (SOC), $MnSb_2Te_4$ is a semiconductor with a direct band gap of $E_{\rm g} \sim 0.09\,{\rm eV}$ [Fig. 4(a)]. When SOC is

TABLE I. Crystallographic data for $MnSb_2Te_4$ obtained from XRD at room temperature (upper) and PND at 50-K (lower) data. The assumed space group is $R3m$ with $a = 4.2385(3)$ Å and $c = 40.8497(3)$ Å from XRD and $a = 4.2219(2)$ Å and $c = 40.606(3)$ Å from PND. g represents the occupancy factor of each site, and U_{iso} employs an overall Debye-Waller factor.

Atom	Site	g^b	x	Y	z	$U_{iso}/100$ Å^2
Mn1	3*a*	0.6645(3)	0	0	0	1.62(3)
		0.666(7)				0. 6(1)
Sb1	3*a*	0.3355(3)	0	0	0	1.62(3)
		0.333(7)				0.6(1)
Sb2	6*c*	0.8323(3)	0	0	0.42802(15)	1.62(3)
		0.833(4)			0.4254(2)	0.6(1)
Mn2	6*c*	0.1677(3)	0	0	0.424802(15)	1.62(3)
		0.167(4)			0.4254(2)	0.6(1)
Te1	6*c*	1	0	0	0.131456(12)	1.06(3)
					0.13160(11)	0.6(1)
Te2	6*c*	1	0	0	0.292259(14)	1.29(3)
					0.29175(13)	0.6(1)

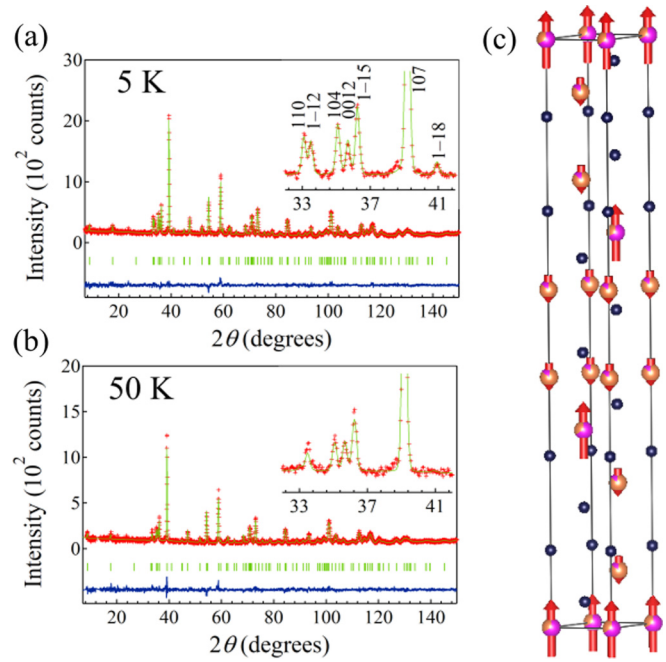

FIG. 5. PND patterns of $MnSb_2Te_4$ at (a) 5 K and (b) 50 K. Red crosses and green and blue lines represent observed, calculated, and difference profiles. Green ticks are used to show the positions of the Bragg peaks. (c) Proposed magnetic structure obtained from 5-K data.

turned on [Fig. 4(b)], we found for the first time a clear band inversion around the Γ point, forming a pair of band crossings along the Γ-Z line. The resultant Weyl cones are tilted with respect to the Γ-Z line, a characteristic feature of type-II Weyl points. From the observed spontaneous magnetization, we deduce that $MnSb_2Te_4$ is a potential TRS broken type-II Weyl semimetal at zero magnetic field.

It is noticed, however, that without SOC the antiferromagnetic (A-type) structure is more stable than the ferromagnetic one by 18.3 meV, similarly to the previous result [38], and inclusion of SOC hardly affects the relative energy difference (17.5 meV). The discrepancy from the ferromagnetic ground state is also inferred from the Curie-Weiss fitting for the susceptibility that yielded a negative Weiss temperature of $\Theta_W = -21.6(4)$ K) [Fig. 2(a)]. Furthermore, the saturation magnetization of about 1.8 μ_B/Mn at 5 K is somewhat smaller than that expected from high-spin Mn^{2+}.

These contradictory observations led us to investigate the structural details of $MnSb_2Te_4$. A structural refinement was initially carried out assuming the ideal $MnBi_2Te_4$-type structure ($R3m$), which, however, resulted in rather poor reliability factors (e.g., $R_{wp} \sim 11\%$) (Fig. S2 in the Supplemental Material [39]). Thus, site mixing among cations was considered in the analysis by allowing Sb (6*c*) to occupy the Mn (3*a*) site and vice versa, while the total occupancy factors were constrained to unity. This substantially improved the fitting [Goodness of fit (GOF) = 1.77, $R_{wp} = 4.51\%$, and $R_p = 1.77\%$] and gave the chemical composition of $(Mn_{0.66}Sb_{0.34})(Sb_{0.83}Mn_{0.17})_2Te_4$. No site deficiency was found for the anionic sites. The full structural parameters are shown in Table I. Cation antisite disorder also occurs in other MPn_2Te_4-type compounds with a site mixing ranging from 15 to 35% [47,48].

We refined the PND data to clarify the effect of site mixing on the magnetism. Above T_C (at 50 K), the refined crystal structure is fully consistent with that obtained from the room-temperature XRD (Table I). At 5 K, we considered various magnetic structures including the ferromagnetic structure to account for the increased nuclear reflections. The best result with $R_{wp} = 8.38\%$ [Fig. 5(a)] was obtained for the ferrimagnetic structure, where the interexchanged Mn atoms at the 6*c* site align antiparallelly along the *c* axis with respect to Mn atoms at the *original* 3*a* site. Magnetic moments are 4.3(2) μ_B and 3.1(3) μ_B for 3*a* and 6*c* sites, respectively. The sublattice magnetic moment of Mn is 2.1 μ_B per unit cell, which is indeed in good accordance with the saturation magnetization value at 5 K [Fig. 2(b)].

The effect of site mixing between Mn and Sb sites was considered for theoretical calculations (see Fig. S3 in the Supplemental Material [39]). Here, we used two site-mixing patterns with a $\sqrt{3} \times \sqrt{3} \times 1$ supercell and calculated the ferromagnetic, ferrimagnetic, and antiferromagnetic spin configurations along the [001] direction. In all the cases, we found magnetic moments only at the Mn atoms. The calculated relative energies are summarized in Table S1 in the Supplemental Material. In the antiferromagnetic case, there are two choices for the magnetic moment of Mn atoms in the Sb layer so we considered their average. As opposed to the disorder-free configuration as described above, the ferrimagnetic structure was found to be most stable. This indicates that the site mixing alters the interlayer exchange coupling from antiferromagnetic to ferromagnetic. We note that the band structures of the ferrimagnetic structures have a band gap. Since these band structures highly depend on the site-mixing patterns, we speculate that a fully random antisite mixing, if achieved, will recover the original crystal structure symmetry and the Weyl-semimetal phase may appear.

IV. CONCLUSION

To summarize, we have synthesized a layered chalcogenide $MnSb_2Te_4$ and measured its fundamental physical properties. The observed spontaneous magnetization below 25 K, differing from the antiferromagnetic order in $MnBi_2Te_4$, can be explained in terms of the ferrimagnetic order where the interexchanged Mn moments are antiparallelly coupled with the original Mn moments. First-principles calculations show that the introduction of antisite disorder plays a key role for the ferromagnetic interaction between Mn layers, which we believe is an important step toward the TRS broken type-II Weyl semimetal state. It should be noted that the Sb sample used here is in a polycrystalline form, which may hamper the observation of the expected topological properties. For further analyses of the topological state in $MnSb_2Te_4$, growth of a single crystal is required, which is in progress. The known MPn_2Te_4 compounds have been predicted to have topological states including the topological insulator, antiferromagnetic topological insulator, and topological axion state [35–37]. We demonstrate here that $MnSb_2Te_4$ represents an example in this family possessing the interlayer ferromagnetic interaction, which warrants further development of topological physics.

ACKNOWLEDGMENTS

This work was supported by a CREST project and Grant-in-Aid for Scientific Research on Innovative Areas, "Mixed anion" (Grants No. 16H6439, No. 16H6440, No. 17H05473, and No. 19H04683), and a Grant-in-Aid for Scientific Research (Grants No. 16H04007 and No. 17H06137) from Ministry of Education, Culture, Sports, Science and Technology. T.M. was supported by Japan Society for the Promotion of Science for Young Scientists.

[1] H. Weng, X. Dai, and Z. Fang, J. Phys. Condens. Matter **28**, 303001 (2016).
[2] B. Yan and C. Felser, Annu. Rev. Condens. Matter Phys. **8**, 337 (2016).
[3] L. M. Schoop, F. Pielnhofer, and B. V. Lotsch, Chem. Mater. **30**, 3155 (2018).
[4] N. P. Armitage, E. J. Mele, and A. Vishwanath, Rev. Mod. Phys. **90**, 015001 (2018).
[5] A. Bernevig, H. Weng, Z. Fang, and X. Dai, J. Phys. Soc. Japan **87**, 041001 (2018).
[6] Z. K. Liu, B. Zhou, Y. Zhang, Z. J. Wang, H. M. Weng, D. Prabhakaran, S. Mo, Z. X. Shen, Z. Fang, X. Dai, Z. Hussain, and Y. L. Chen, Science **343**, 864 (2014).
[7] S. Borisenko, Q. Gibson, D. Evtushinsky, V. Zabolotnyy, B. Büchner, and R. J. Cava, Phys. Rev. Lett. **113**, 027603 (2014).
[8] S. Jeon, B. B. Zhou, A. Gyenis, B. E. Feldman, I. Kimchi, A. C. Potter, Q. D. Gibson, R. J. Cava, A. Vishwanath, and A. Yazdani, Nat. Mater. **13**, 851 (2014).
[9] J. Xiong, S. K. Kushwaha, T. Liang, J. W. Krizan, M. Hirschberger, W. Wang, R. J. Cava, and N. P. Ong, Science **350**, 413 (2015).
[10] X. Huang, L. Zhao, Y. Long, P. Wang, D. Chen, Z. Yang, H. Liang, M. Xue, H. Weng, Z. Fang, X. Dai, and G. Chen, Phys. Rev. X **5**, 031023 (2015).
[11] S. A. Parameswaran, T. Grover, D. A. Abanin, D. A. Pesin, and A. Vishwanath, Phys. Rev. X **4**, 031035 (2014).
[12] L. X. Yang, Z. K. Liu, Y. Sun, H. Peng, H. F. Yang, T. Zhang, B. Zhou, Y. Zhang, Y. F. Guo, M. Rahn, D. Prabhakaran, Z. Hussain, S. K. Mo, C. Felser, B. Yan, and Y. L. Chen, Nat. Phys. **11**, 728 (2015).
[13] C. Shekhar, A. K. Nayak, Y. Sun, M. Schmidt, M. Nicklas, I. Leermakers, U. Zeitler, Y. Skourski, J. Wosnitza, Z. Liu, Y. Chen, W. Schnelle, H. Borrmann, Y. Grin, C. Felser, and B. Yan, Nat. Phys. **11**, 645 (2015).
[14] Z. K. Liu, L. X. Yang, Y. Sun, T. Zhang, H. Peng, H. F. Yang, C. Chen, Y. Zhang, Y. F. Guo, D. Prabhakaran, M. Schmidt, Z. Hussain, S. K. Mo, C. Felser, B. Yan, and Y. L. Chen, Nat. Mater. **15**, 27 (2016).
[15] K. Kuroda, T. Tomita, M. T. Suzuki, C. Bareille, A. A. Nugroho, P. Goswami, M. Ochi, M. Ikhlas, M. Nakayama, S. Akebi, R. Noguchi, R. Ishii, N. Inami, K. Ono, H. Kumigashira, A. Varykhalov, T. Muro, T. Koretsune, R. Arita, S. Shin, T. Kondo, and S. Nakatsuji, Nat. Mater. **16**, 1090 (2017).
[16] E. Liu, Y. Sun, N. Kumar, L. Muechler, A. Sun, L. Jiao, S. Y. Yang, D. Liu, A. Liang, Q. Xu, J. Kroder, V. Süß, H. Borrmann, C. Shekhar, Z. Wang, C. Xi, W. Wang, W. Schnelle, S. Wirth, Y. Chen, S. T. B. Goennenwein, and C. Felser, Nat. Phys. **14**, 1125 (2018).
[17] A. A. Soluyanov, D. Gresch, Z. Wang, Q. Wu, M. Troyer, X. Dai, and B. A. Bernevig, Nature (London) **527**, 495 (2015).
[18] A. A. Zyuzin and R. P. Tiwari, JETP Lett. **103**, 717 (2016).
[19] Y. Wu, D. Mou, N. H. Jo, K. Sun, L. Huang, S. L. Bud'ko, P. C. Canfield, and A. Kaminski, Phys. Rev. B **94**, 121113(R) (2016).
[20] K. Deng, G. Wan, P. Deng, K. Zhang, S. Ding, E. Wang, M. Yan, H. Huang, H. Zhang, Z. Xu, J. Denlinger, A. Fedorov, H. Yang, W. Duan, H. Yao, Y. Wu, S. Fan, H. Zhang, X. Chen, and S. Zhou, Nat. Phys. **12**, 1105 (2016).
[21] Z. Wang, D. Gresch, A. A. Soluyanov, W. Xie, S. Kushwaha, X. Dai, M. Troyer, R. J. Cava, and B. A. Bernevig, Phys. Rev. Lett. **117**, 056805 (2016).
[22] A. Tamai, Q. S. Wu, I. Cucchi, F. Y. Bruno, S. Riccò, T. K. Kim, M. Hoesch, C. Barreteau, E. Giannini, and C. Besnard, A. A. Soluyanov, and F. Baumberger, Phys. Rev. X **6**, 031021 (2016).
[23] I. Belopolski, P. Yu, D. S. Sanchez, Y. Ishida, T. R. Chang, S. S. Zhang, S. Y. Xu, H. Zheng, G. Chang, G. Bian, H. T. Jeng, T. Kondo, H. Lin, Z. Liu, S. Shin, and M. Z. Hasan, Nat. Commun. **8**, 942 (2017).
[24] E. Haubold, K. Koepernik, D. Efremov, S. Khim, A. Fedorov, Y. Kushnirenko, J. van den Brink, S. Wurmehl, B. Büchner, T. K. Kim, M. Hoesch, K. Sumida, K. Taguchi, T. Yoshikawa, A. Kimura, T. Okuda, and S. V. Borisenko, Phys. Rev. B **95**, 241108(R) (2017).
[25] H. Zheng, H. Lin, T. Neupert, Y. Bian, M.-A. Husanu, C.-H. Hsu, H. Lu, I. Belopolski, A. Bansil, G. Chang, M. Z. Hasan, D. S. Sanchez, X. Zhang, N. Alidoust, B. Singh, S. Jia, V. N.

Strocov, S.-Y. Xu, G. Bian, S.-M. Huang, H.-T. Jeng, and T.-R. Chang, Sci. Adv. **3**, e1603229 (2017).
[26] S. Borisenko, D. Evtushinsky, Q. Gibson, A. Yaresko, T. Kim, M. N. Ali, B. Buechner, M. Hoesch, and R. J. Cava, arXiv:1507.04847.
[27] D. Chaudhuri, B. Cheng, A. Yaresko, Q. D. Gibson, R. J. Cava, and N. P. Armitage, Phys. Rev. B **96**, 075151 (2017).
[28] G. Chang, B. Singh, S. Y. Xu, G. Bian, S. M. Huang, C. H. Hsu, I. Belopolski, N. Alidoust, D. S. Sanchez, H. Zheng, H. Lu, X. Zhang, Y. Bian, T. R. Chang, H. T. Jeng, A. Bansil, H. Hsu, S. Jia, T. Neupert, H. Lin, and M. Z. Hasan, Phys. Rev. B **97**, 041104(R) (2018).
[29] L. A. Kuznetsova, V. L. Kuznetsov, and D. M. Rowe, J. Phys. Chem. Solids **61**, 1269 (2000).
[30] S. Kuypers, G. Van Tendeloo, J. Van Landuyt, and S. Amelinckx, Micron Microsc. Acta **18**, 245 (2002).
[31] D. S. Lee, T. H. Kim, C. H. Park, C. Y. Chung, Y. S. Lim, W. S. Seo, and H. H. Park, Cryst. Eng. Comm. **15**, 5532 (2013).
[32] A. M. Essin and V. Gurarie, Phys. Rev. B **85**, 195116 (2012).
[33] M. M. Otrokov, I. P. Rusinov, M. Blanco-Rey, M. Hoffmann, A. Y. Vyazovskaya, S. V. Eremeev, A. Ernst, P. M. Echenique, A. Arnau, and E. V. Chulkov, Phys. Rev. Lett. **122**, 107202 (2019).
[34] D. Zhang, M. Shi, T. Zhu, D. Xing, H. Zhang, and J. Wang, Phys. Rev. Lett. **122**, 206401 (2019).
[35] M. M. Otrokov, I. I. Klimovskikh, H. Bentmann, A. Zeugner, Z. S. Aliev, S. Gass, A. U. B. Wolter, A. V Koroleva, D. Estyunin, and A. M. Shikin, arXiv:1809.07389.
[36] Y. Gong, J. Guo, J. Li, K. Zhu, M. Liao, X. Liu, Q. Zhang, L. Gu, L. Tang, and X. Feng, Chin. Phys. Lett. **36**, 076801 (2019).
[37] B. Chen, F. Fei, D. Zhang, B. Zhang, W. Liu, S. Zhang, P. Wang, B. Wei, Y. Zhang, and J. Guo, Nat. Commun. **10**, 4469 (2019).
[38] S. V. Eremeev, M. M. Otrokov, and E. V. Chulkov, J. Alloys Compd. **709**, 172 (2017).
[39] See Supplemental Material at http://link.aps.org/supplemental/10.1103/PhysRevB.100.195103 for more details on analyses for XRD and PND data, theoretical calculations, and specific-heat measurements.
[40] G. Kresse and J. Furthmüller, Phys. Rev. B **54**, 11169 (1996).
[41] G. Kresse and J. Furthmüller, Comput. Mater. Sci. **6**, 15 (1996).
[42] V. Petříček, M. Dušek, and L. Palatinus, Z. Krist. Mater. **229**, 345 (2014).
[43] J. Rodríguez-Carvajal, Phys. B **192**, 55 (1993).
[44] J.-Q. Yan, Q. Zhang, T. Heitmann, Zengle Huang, K. Y. Chen, J.-G. Cheng, Weida Wu, D. Vaknin, B. C. Sales, and R. J. McQueeney, Phys. Rev. Materials **3**, 064202 (2019).
[45] E. J. J. Mallmann, A. S. B. Sombra, J. C. Goes, and P. B. A. Fechine, Solid State Phenom. **202**, 65 (2013).
[46] M. M. Otrokov, I. I. Klimovskikh, H. Bentmann, A. Zeugner, Z. S. Aliev, S. Gass, A. U. B. Wolter, A. V. Koroleva, D. Estyunin, A. M. Shikin, M. Blanco-Rey, M. Hoffmann, A. Y. Vyazovskaya, S. V. Eremeev, Y. M. Koroteev, I. R. Amiraslanov, M. B. Babanly, N. T. Mamedov, N. A. Abdullayev, V. N. Zverev, B. Büchner, E. F. Schwier, S. Kumar, A. Kimura, L. Petaccia, G. Di Santo, R. C. Vidal, S. Schatz, K. Kißner, C.-H. Min, S. K. Moser, T. R. F. Peixoto, F. Reinert, A. Ernst, P. M. Echenique, A. Isaeva, and E. V. Chulkov, arXiv:1809.07389.
[47] B. A. Kuropatwa and H. Kleinke, Z. Anorg. Allg. Chem. **638**, 2640 (2012).
[48] A. Zeugner, F. Nietschke, A. U. B. Wolter, S. Gaß, R. C. Vidal, T. R. F. Peixoto, D. Pohl, C. Damm, A. Lubk, R. Hentrich, S. K. Moser, C. Fornari, C. H. Min, S. Schatz, K. Kißner, M. Ünzelmann, M. Kaiser, F. Scaravaggi, B. Rellinghaus, K. Nielsch, C. Hess, B. Büchner, F. Reinert, H. Bentmann, O. Oeckler, T. Doert, M. Ruck, and A. Isaeva, Chem. Mater. **31**, 2795 (2019).